

Electron paramagnetic resonance study of ErSc₂N@C₈₀

Rizvi Rahman^{*,1,†}, Archana Tiwari^{*,2}, Géraldine Dantelle³, John J. L. Morton^{1,4,‡},
Kyriakos Porfyrakis¹, Arzhang Ardavan⁴, Klaus-Peter Dinse⁵, and G. Andrew D. Briggs¹

¹*Department of Materials, Oxford University, Oxford OX1 3PH, UK*

²*Department of Physical Sciences, Sikkim University, Gangtok 737102, India*

³*Laboratoire de Physique de la Matière Condensée CNRS UMR 7643 Ecole Polytechnique,
Route de Saclay, 91128 Palaiseau Cedex, France*

⁴*CAESR, Clarendon Laboratory, Dept. of Physics, Oxford University, Oxford OX1 3PU, UK*

⁵*Freie Universität Berlin, Fachbereich Physik, Arnimallee 14 14195 Berlin, Germany*

(Dated: June 12, 2022)

We present an electron paramagnetic resonance (EPR) study of ErSc₂N@C₈₀ fullerene in which there are two Er³⁺ sites corresponding to two different configurations of the ErSc₂N cluster inside the C₈₀ cage. For each configuration, the EPR spectrum is characterized by a strong anisotropy of the g -factors ($g_{x,y} = 2.9$, $g_z = 13.0$ and $g_{x,y} = 5.3$, $g_z = 10.9$). Illumination within the cage absorption range ($\lambda < 600$ nm) induces a rearrangement of the ErSc₂N cluster inside the cage. We follow the temporal dependence of this rearrangement phenomenologically under various conditions.

INTRODUCTION

Rare-earth (RE) doped fullerenes have been widely studied because of their interesting structural, magnetic and optical properties [1–3]. Many studies investigate optical properties and are devoted to the determination of the electronic structure of the RE ions inside the cage [1, 4–6]. However, there is a smaller number of reports about the ground-state spin characteristics of the doped ions, which can be examined by electron paramagnetic resonance (EPR) [7, 8]. The combination of EPR and optical spectroscopy offers a powerful approach to understanding the electronic structure and local symmetries of the ion.

Photoluminescence (PL) has previously been reported from the Er³⁺ ion in ErSc₂N@C₈₀ around 1.5 μm [3, 9, 10], revealing that the ErSc₂N cluster inside the C₈₀ cage occupies two dominant spatial configurations, corroborating earlier X-ray crystallographic studies [11]. At low temperatures, one of the configurations is favoured over the other, and illumination with visible light was found to switch the ErSc₂N molecular cluster inside the cage from one configuration to the other [12].

In this article we report a detailed EPR investigation of ErSc₂N@C₈₀, including a study on the switching of two configurations of the ErSc₂N cluster within the cage.

MATERIALS AND METHODS

ErSc₂N@C₈₀ was purchased from Luna Innovations with an approximate purity of 60%. Impurities included other erbium doped metallofullerenes. It was further purified to >95% by high performance liquid chromatogra-

phy (HPLC). Solutions were prepared in toluene (>99%, Fisher Scientific) and *o*-terphenyl (99% Aldrich) with a minimum concentration of 3×10^{-4} M (approximately 10^{15} ErSc₂N@C₈₀ molecules). The solution was freeze-pumped in liquid nitrogen for several cycles to deoxygenate the solvent and was sealed under vacuum in a 4 mm quartz EPR tube. CW EPR spectra were recorded in the temperature range 5 K to 30 K using an X-band Bruker EMX Micro EPR spectrometer equipped with a rectangular TE₁₀₂ cavity (quality factor of about 12000) with an optical window and an Oxford ESR900 helium flow cryostat. The sample was illuminated using a range of sources: a Nd:YAG laser ($\lambda = 532$ nm); a tunable infra-red laser ($\lambda = 1420 - 1520$ nm); and light emitting diodes (LEDs) of 10 mW power emitting at 400 nm, 470 nm and 525 nm. Throughout, the microwave frequency was 9.4 GHz. The magnetic field was swept in the range 0 to 400 mT, modulated with an amplitude of 0.3 mT at a frequency of 100 kHz.

EPR SPECTRA AND THE HYPERFINE STRUCTURE

Assuming a completely ionic model, the electronic configuration of ErSc₂N@C₈₀ can be written as Er³⁺(Sc³⁺)₂N³⁻@C₈₀⁶⁻ [5]. Sc³⁺, N³⁻ and C₈₀⁶⁻ have no unpaired electrons, whereas the Er³⁺ ion, with $4f^{11}$ electrons in its valence shell, is presumably the only EPR-active species inside ErSc₂N@C₈₀. Erbium has six natural isotopes, ¹⁶²Er, ¹⁶⁴Er, ¹⁶⁶Er, ¹⁶⁷Er, ¹⁶⁸Er and ¹⁷⁰Er. Only ¹⁶⁷Er, with a natural abundance of 23%, has an effective nuclear spin $I = 7/2$. The other isotopes have $I = 0$. EPR of rare-earth (RE) ions in a weak crystal-field is normally observed only at low temperatures, owing to fast spin-lattice relaxation [13]. At 5 K, only the lowest doublet is expected to be populated giving rise to the resonance spectrum with an effective spin $S_{\text{eff}} = 1/2$.

*Both authors contributed equally to this work

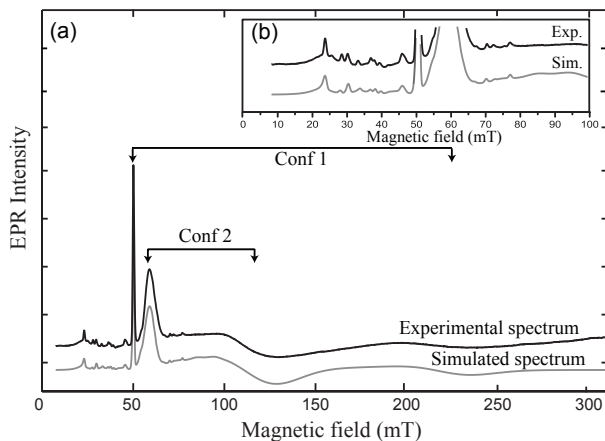


FIG. 1: (a) X-band CW EPR spectrum of $\text{ErSc}_2\text{N}@C_{80}$ in a frozen toluene solution at 5 K and EasySpin simulated spectrum. (b) Expanded spectra of the experimental and simulated curves in the low-field region showing the resolved hyperfine splitting.

TABLE I: Simulated principal values of g and A (in MHz) of Er^{3+} in $\text{ErSc}_2\text{N}@C_{80}$ for *Conf 1* and *Conf 2*. The A_x and A_y values and the components of Q (in MHz) are only reported for Er^{3+} in *Conf 1*; for Er^{3+} in *Conf 2*, the effect of these values remains unresolved.

Axis	Er^{3+} , <i>Conf 1</i>			Er^{3+} , <i>Conf 2</i>	
	g	A	Q	g	A
x	2.9 (0.3)	380 (50)	10 (5)	5.3 (0.3)	NA
y	2.9 (0.3)	380 (50)	130 (5)	5.3 (0.3)	NA
z	13.0 (0.1)	1380 (10)	10 (2)	10.9 (0.1)	1590 (20)

The EPR spectrum of $\text{ErSc}_2\text{N}@C_{80}$ in toluene was only observed at temperatures below 30 K. The spectrum of $\text{ErSc}_2\text{N}@C_{80}$ in toluene at 5 K is shown in Figure 1. EPR peaks, at 51 mT and 220 mT and at 60 mT and 110 mT, are attributed to two non-equivalent Er^{3+} ions inside the cage, corresponding to two orientation of the internal cluster within the molecule [12]. Additional hyperfine structure is also observed around the narrow low-field lines. EasySpin software [14] was used to simulate the experimental spectrum, with an effective spin-Hamiltonian:

$$H_{\text{eff}} = \mu_B g B \cdot S_{\text{eff}} + \mu_n g_n B \cdot I + S_{\text{eff}} \cdot A \cdot I + I \cdot Q \cdot I \quad (1)$$

where the four terms correspond to the electron- and nuclear spin Zeeman interaction, the hyperfine interaction and the nuclear-quadrupolar interaction respectively.

The simulated spectrum, as shown in Figure 1, reproduces the experimental one accurately. The relative intensities of the EPR peaks are simulated using the natural Er isotopic abundance. The simulation parameters are given in Table I. The g -, A - and Q -tensors are characterised by one large and two small components, revealing the large anisotropy in the system. We extract a set of

values for Er^{3+} in each of the two configurations in $\text{ErSc}_2\text{N}@C_{80}$. Owing to the narrow linewidth (0.8 mT) of the transition at 51 mT for *Conf 1*, further splitting caused by the nuclear-quadrupolar interaction Q was observed. However, for the other configurations, *Conf 2*, the values of A_x and A_y could not be determined accurately because of the large linewidths and the low intensities of the corresponding peaks of *Conf 2*. Similarly, the effect of the quadrupolar interaction is smeared out over the respective hyperfine lines.

The results of Table I seem to suggest an axial symmetry for the tensors. However, from previous X-ray diffraction measurements the planar ErSc_2N cluster has been found to possess a C_{2v} (or orthorhombic) symmetry [11]. In addition, the Er^{3+} ion sits probably in an even lower symmetry site if one considers the neighbouring carbon atoms of the C_{80} cage, which are located 2.5 to 3 Å from the ion [11]. Since the uncertainties obtained from our fitting of the g -, A - and Q -tensors are relatively large, we then conclude that these tensors have in fact no particular symmetry.

The values of the ratios A_x/g_x , A_y/g_y and A_z/g_z for *Conf 1* are not equal. This means that the crystal field admixes significant amounts of different $\{J, m_J\}$ states to the ground state [13]. The presence of such admixtures has also been shown in the closely related $\text{Er}_3\text{N}@C_{80}$ fullerene from photoluminescence spectroscopy and crystal-field modelling [15]. It is interesting that the results obtained by Guillot-Noel *et al.* for Er:YSO crystals where the Er sits in C_1 symmetry sites, give similar values for the hyperfine parameters and thus, significant mixing between $\{J, m_J\}$ states [16].

As another consequence of the low symmetry of the Er^{3+} in $\text{ErSc}_2\text{N}@C_{80}$, the Q tensor axes are not coincident with respect to the g and A tensors [17]. The high Q_y value is about the same order of magnitude as the x and y components of the hyperfine tensor, thus making nuclear electric quadrupole transitions observable in the EPR spectrum as additional satellite peaks near the intense 51 mT peak.

It is extremely difficult to obtain more structural information from all the tensor values as the EPR spectrum is a powder spectrum, further complicated by the presence of two configurations whose linewidths are very different. Further information could be obtained by aligning these molecules, for example with a high magnetic field (some magnetic orientation has been shown on $\text{Er}_3\text{N}@C_{80}$ in CS_2 with a field of 19 T [15, 18]) and study the EPR spectra at various sample rotation angle.

LINE BROADENING

At low temperatures, the EPR linewidth $\delta\omega$ is affected by inhomogeneities in the sample such as the g - and A -strains, unresolved hyperfine couplings, and also by

homogeneous effects which limit the linewidths to $1/T_2$, where T_2 is the spin-spin relaxation time [19]. As the temperature rises, the spin-lattice relaxation time (T_1) shortens, limiting T_2 and leading to broadening of EPR peaks.

Figure 2 shows EPR spectra of $\text{ErSc}_2\text{N}@C_{80}$ at different temperatures. The inset shows the evolution of linewidths of the peaks at 51 mT and 60 mT as a function of $1/T$, which fit well to the general expression of the form:

$$\delta\omega = \frac{S}{[\exp(\frac{\Delta_E}{k_B T}) - 1]} + \text{Constant} \quad (2)$$

where k_B is the Boltzmann constant, S is the magnitude of the linewidth normalized by the phonon occupation number and Δ_E is the energy of an excited level. This dependence reflects that the spin-lattice relaxation is an Orbach mechanism, i.e. a two phonon T_1 process where the relaxation takes place via an excited state [20].

The energy Δ_E , obtained from the fitting parameters of Equation (2) for the two peaks at 51 mT and 60 mT, is found to be $36(1) \text{ cm}^{-1}$ and $25(4) \text{ cm}^{-1}$, respectively. PL spectroscopy has previously revealed the crystal-field energy levels of the Er^{3+} ion in two different configurations, corresponding to two different orientations of the ErSc_2N cluster within the C_{80} cage [9]. The energy difference between the lowest and second lowest crystal-field levels of the ground state $^4I_{15/2}$ of Er^{3+} ion is 37 cm^{-1} for *Conf 1* and 28 cm^{-1} for *Conf 2*. Δ_E , deduced from the EPR studies, is in good agreement with the energy dif-

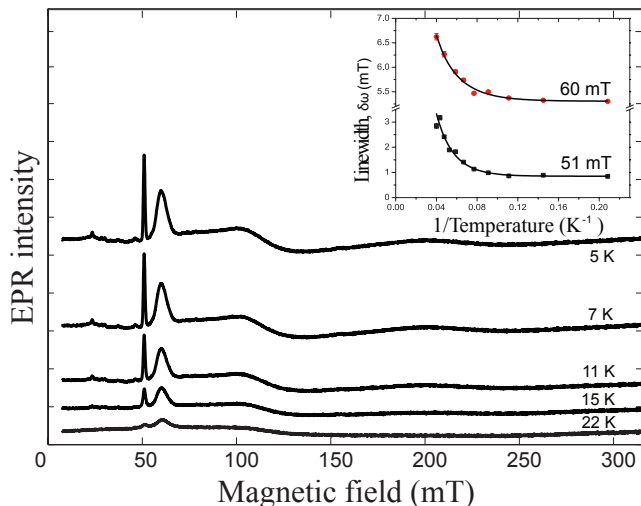


FIG. 2: EPR spectra of $\text{ErSc}_2\text{N}@C_{80}$ at different temperatures. The inset shows the temperature dependence of linewidths of two most intense peaks at 51 mT and 60 mT observed in the EPR spectrum at 5 K. The symbols and the solid curves indicate the experimental data and the fitted curve, respectively. The activation energy calculated from fitting the evolution of $\delta\omega$ as a function of temperature support the assignment of these peaks to *Conf 1* and *Conf 2* respectively.

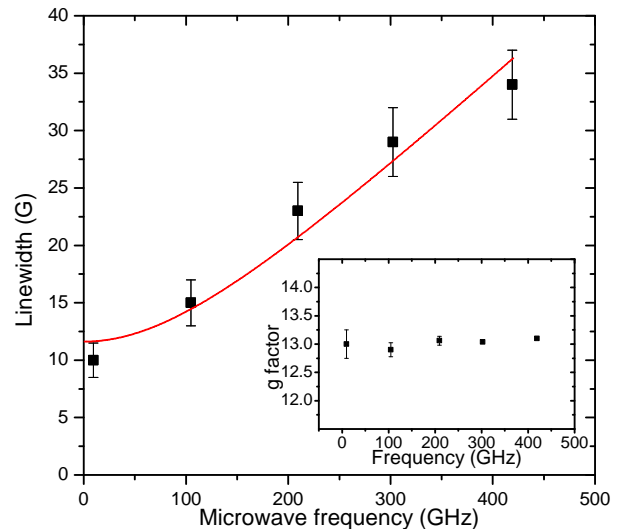


FIG. 3: Linewidth and g -factor (inset) of g_z feature of *Conf 1* as a function of microwave frequency. The solid line is a fit to a combination of a frequency-independent homogeneous component to the linewidth (12 G), and a g -strain component which is linear with frequency (82 mG/GHz).

ferences obtained in PL. Thus, EPR peaks at 51 mT and 60 mT are assigned to the optically observed ErSc_2N configurations, *Conf 1* and *Conf 2*, respectively.

HIGH-FREQUENCY EPR

High frequency CW-EPR of $\text{ErSc}_2\text{N}@C_{80}$ was performed at the National High Magnetic Field Lab (NHMFL), Tallahassee using their home-built 100–600 GHz homodyne spectrometer [21]. Figure 3 shows the linewidth dependence of the narrowest spectral feature, the g_z feature of *Conf 1*, as a function of microwave frequency (and thus magnetic field). The data are consistent with the linewidth at X-band (10 GHz) being homogeneously broadened (on which assumption the analysis above relied), while at higher frequency g -strain across the sample causes a linear increase in linewidth. The g -strain which can be extracted is small: $\approx 0.15\%$ indicating its value shows a very weak dependence on local environment.

EPR SPECTRA UPON ILLUMINATION

Wavelength dependence

In this section we discuss the influence of optical illumination on the EPR spectrum of $\text{ErSc}_2\text{N}@C_{80}$. For each excitation wavelength, the sample was illuminated for 20 mins at 5 K before the EPR spectrum was recorded. Between measurements at different wavelengths, the

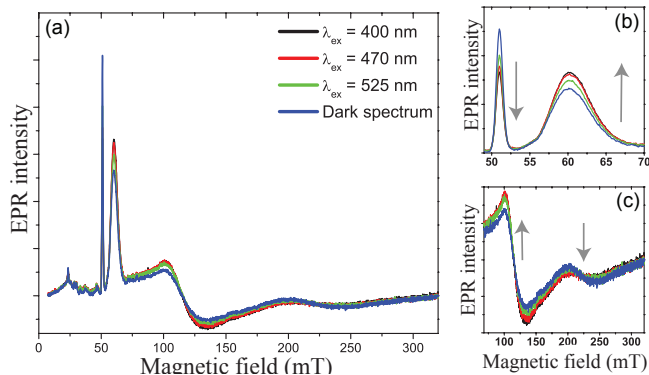


FIG. 4: (a) Influence of illumination at 400 nm, 470 nm and 525 nm on the EPR signal of Er^{3+} ion in $\text{ErSc}_2\text{N}@C_{80}$ in toluene at 5 K. The figures (b) and (c) show changes in the peak intensities at 51 mT and 60 mT, and 220 mT and 110 mT. For a comparison, the EPR spectrum of a non-illuminated sample is also shown.

sample was heated above 35 K and then cooled down to 5 K. This annealing process provided the same initial conditions before each new period of illumination.

Initially, we illuminated the Er^{3+} ions to excite transitions within the crystal-field levels directly, using excitation wavelengths of 1496 nm and 1499 nm [9] for *Conf 1* and *Conf 2* respectively. These wavelengths are too long to excite the cage and had no effect on the EPR spectrum.

We then excited $\text{ErSc}_2\text{N}@C_{80}$ at different wavelengths well within the cage absorption range using 400 nm, 470 nm and 525 nm LEDs. The EPR spectra of $\text{ErSc}_2\text{N}@C_{80}$ under LED illumination are shown in Figure 4. For comparison, the EPR spectrum without illumination is also shown on the same graph. The spectra reveal that the intensities of the EPR peaks corresponding to the two ErSc_2N configurations ions vary in opposite directions (indicated by the arrows), allowing the assignment of the set of peaks at 51 mT and 220 mT to *Conf 1* and the set of 60 mT and 110 mT peaks to the other *Conf 2* [12]. The line shape and spin-Hamiltonian parameters remain unchanged on illumination, and no evolution of any new spectral features is observed.

The change in the EPR intensity for each configuration indicates that the ErSc_2N cluster rearranges within the C_{80} cage upon illumination. Exciting $\text{ErSc}_2\text{N}@C_{80}$ with visible light appears to preferentially drive the switching one configuration to the other. As the direct excitation of Er^{3+} ion has no influence on the relative proportion of the two configurations, we can conclude that the configurational changes are mediated via the cage. Subsequently, we used a green laser operating at 532 nm as an excitation source. The resulting change in the EPR spectrum was consistent with the effect of illumination using LEDs. Probably owing to the higher excitation power (26 mW, compared to 10 mW for the LEDs), illumina-

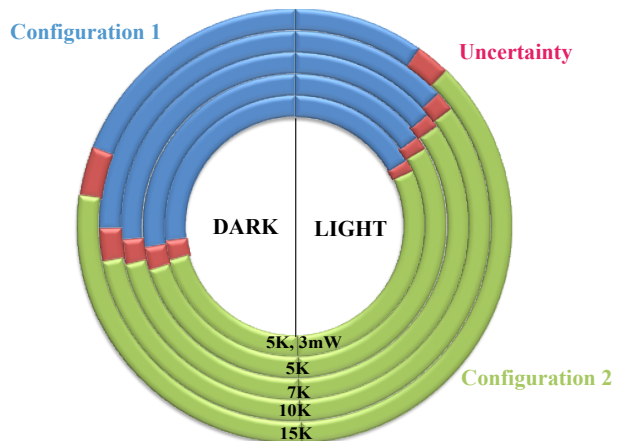


FIG. 5: Populations of *Conf 1* and *Conf 2* from the ESR peaks of $\text{ErSc}_2\text{N}@C_{80}$ in o-terphenyl for various experimental conditions. The excitation laser was set to 532 nm and 20 mW power, except for one measurement as indicated in the figure. The sample was annealed at room temperature between each measurement.

tion with the 532 nm laser induced a 10% larger change in the EPR intensities as compared to the illumination with the 525 nm LED in the given time span of 20 mins.

Temperature dependence

We studied the effect on the EPR spectrum of laser illumination at 532 nm at various temperatures, T , between 5 K and 15 K. The integrated area of the spectrum depends on many factors, including transition moment, temperature, microwave power and relaxation times. We combine all such terms into a constant of proportionality κ such that the intensity of a feature attributed to *Conf i*, $I_i = \kappa_i n_i$, where n_i is the number of spins in *Conf i*.

Assuming that κ_i for a particular configuration is independent of the illumination, the change in the integrated area under the resonance peak provides a measure of the change in the configuration populations. We examined the resonance peaks at 51 mT and 60 mT corresponding to *Conf 1* and *Conf 2* respectively. Figure 5 shows the change in the populations for *Conf 1* and *Conf 2* at various temperatures with and without illumination. The populations were obtained by a fitting procedure assuming that the total number of spin is constant and that only two configurations are present. The latter assumption has been verified experimentally (see the population switching dynamics section).

Previously, it has been shown that at 5 K a swing in configuration population by as much as $\approx 27\%$ *Conf 2* is possible [12] upon optical illumination. In order to study the effect on switching of various parameters, such as temperature, it is important to control the molecular environment carefully. The use of toluene as a solvent

produces a metastable glass upon freezing which easily cracks and form a polycrystal. In such a polycrystal, the various orientations of the grains induce strains that probably impact on the local environment of the fullerene, and hence the Er^{3+} ions. We therefore used o-terphenyl as a solvent as it is known to produce stable glasses, and therefore a more reproducible environment for the ErSc_2N . In this case, the sample needs to be first heated to about 330 K and then quickly frozen in liquid nitrogen. We observe in figure 5 that the *Conf 2* is predominant at higher temperatures. Moreover, a weaker laser illumination results in less switching of *Conf 1* to *Conf 2*. To summarise, the analysis of the populations before and after illumination shows that higher temperatures and illumination both favour *Conf 2*.

POPULATION SWITCHING DYNAMICS UPON ILLUMINATION

Evidence for the switching between only two configurations ErSc_2N cluster

Here we report the experimental dynamics of the population switching between two configurations of ErSc_2N cluster within the C_{80} cage upon illumination.

The magnetic field range was selected to include the two sharp peaks at 51 mT and 60 mT. The sample was diluted in o-terphenyl as it formed a better glass than toluene. After being kept in dark for about 5 min, it was illuminated with a laser at 532 nm and 20 mW power for 48 min. The changes in EPR peaks at 51 mT and 60 mT were recorded simultaneously.

As the laser is turned on, the intensity of the peak at 51 mT, corresponding to *Conf 1*, decreases and the one for the peak at 60 mT, corresponding to *Conf 2*, increases.

The integrated area (I_i) under the two sharp peaks at 51 mT and 60 mT was calculated for each spectrum. Figure 6(a) shows the temporal evolution of the areas (I_i) before and during illumination.

We assume that the total number of spins $n_1 + n_2 = \frac{I_1}{\kappa_1} + \frac{I_2}{\kappa_2}$ is constant throughout illumination. We test this assumption and derive the ratio of the intensity factor κ_i , by plotting $(\frac{\kappa_2}{\kappa_1} I_1 + I_2)$ as function of time for different ratios of κ_2/κ_1 . Through a fitting procedure we find that for $\kappa_2/\kappa_1 = 3.2 \pm 0.1$, the function $(\frac{\kappa_2}{\kappa_1} I_1 + I_2)$, which is proportional to the total number of spins in *Conf 1* and *Conf 2*, is constant. This is illustrated in Figure 6(b) for a range of $\kappa_2/\kappa_1 = 2.2, 3.2, 4.2$. This value can be approximately understood by considering the different total spectral widths (g_\perp to g_\parallel) of the two configurations.

As $t \rightarrow \infty$, the area under the two peaks corresponding to each configuration, $I_1(\infty)$ and $I_2(\infty)$, reaches a steady regime under a constant illumination (see Figure 6(a)). From Figure 6(a), the ratio $I_1(\infty)/I_2(\infty)$ can be evalu-

ated. As we know that:

$$\frac{I_1(\infty)}{I_2(\infty)} = \frac{n_1(\infty)\kappa_1}{n_2(\infty)\kappa_2} \quad (3)$$

and the ratio $\kappa_2/\kappa_1 = 3.2$, we can deduce the ratio $n_1(\infty)/n_2(\infty)$. At 5 K and 20 mW, the ratio is:

$$\frac{n_1(\infty)}{n_2(\infty)} = 0.45(2) \quad (4)$$

This ratio is in agreement with that reported previously [12]. We note that this shows the light-induced switching observed is not due to sample heating, which would reduce the intensity of both peaks, as shown above.

Effects of temperature and power on the temporal evolution

In order to gain further insight on the switching dynamics, we performed similar time scan measurements at a lower power and higher temperatures. The temporal evolution of the integrated area under various conditions for each configuration is shown in Figure 7. We confirmed that for most conditions, the ratio κ_2/κ_1 for 3 mW is unchanged at 3.2 ± 0.1 . Only at 10 K this ratio is slightly higher, with $\kappa_2/\kappa_1 = 3.8 \pm 0.1$. Thus, we can directly translate the changes in EPR peak areas to the populations dynamics of the configurations.

The data are well fit to biexponential decay functions of time, with a slow decay time (T_s) and a fast decay time (T_f). We consider the average decay time $T_{avg} = (A_s T_s + A_f T_f)$, where A_s and A_f are the normalised amplitudes of the two exponential decay components. The results are presented in Table II. Reducing laser power from 20 to 3 mW has no significant effect on the extracted ratios of $n_1(0)/n_2(0)$ and $n_1(\infty)/n_2(\infty)$, as expected from Figure 5, however the average decay time T_{avg} is much slower.

In contrast, changing the temperature from 5 to 10 K involves a change in both the initial and final population ratios (as observed above). However it does not affect T_{avg} . Thus, the temporal evolution of the switching process is dominated by the kinetic effect of laser power, rather than a thermodynamic effect.

Simple kinetic models involving different excitation and relaxation rates can reproduce the basic form of this biexponential behaviour, however a quantitative comparison would require a detailed understanding of the energy transfer process between the carbon cage and the Er^{3+} ion. Further optical studies on ErSc_2N and related TNT fullerenes will help to elucidate this transfer process and the energy levels involved.

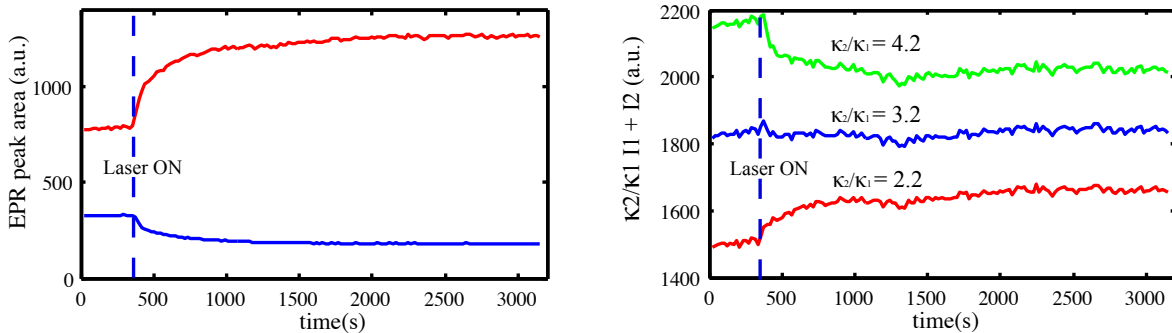


FIG. 6: (a) Temporal evolution of the integrated area under the EPR peaks at 51 mT and 60 mT before and during illumination. Temperature = 5 K; excitation wavelength $\lambda = 532$ nm; power = 20 mW. (b) Plot of $\kappa_2/\kappa_1 * I_1 + I_2$ versus time for $\kappa_2/\kappa_1 = 2.2$, 3.2 and 4.2.

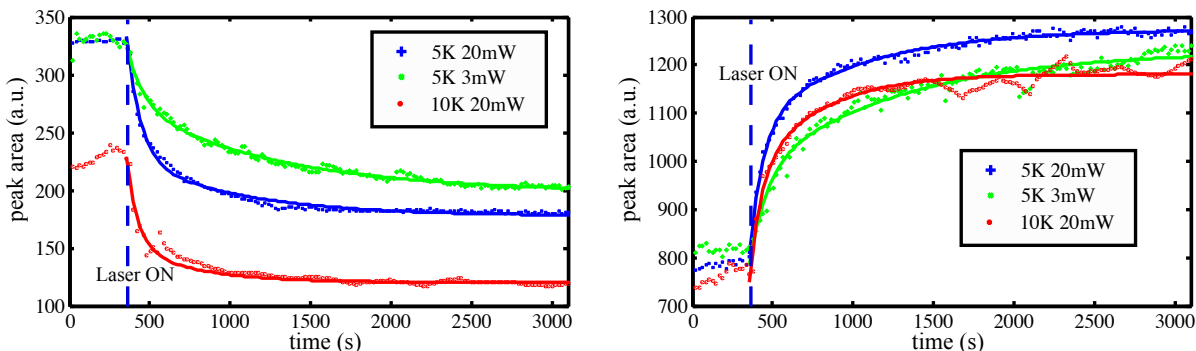


FIG. 7: (a) Time response of the integrated area under the peak at 51 mT before and during illumination at $T = 5$ K and 10 K with an excitation wavelength $\lambda = 532$ nm and power of 20 mW and 3 mW. (b) Time response of the integrated area under the peak at 60 mT before and under illumination at $T = 5$ K and 10 K with an excitation wavelength $\lambda = 532$ nm and a power of 20 mW. The laser was turned on after 400s. Smooth curves show biexponential fits with the parameters from the model.

T (K)	Power (mW)	$\frac{n_1(0)}{n_2(0)}$	$\frac{n_1(\infty)}{n_2(\infty)}$	T_{avg} (s)
5	20	1.33(0.02)	0.45(0.02)	302(60)
5	3	1.28(0.02)	0.50(0.02)	613(100)
10	20	1.12(0.02)	0.37(0.02)	309(60)

TABLE II: Average decay times deduced from the fitting parameters of the bi-exponential temporal evolution of the average integrated area as a function of temperature and laser power.

Relaxation after illumination

When the laser is turned off, the peak intensities evolve in the opposite direction in a monoexponential way. This is consistent with a direct relaxation between *Conf 2* and *Conf 1*. This relaxation is very slow compared to the excitation timescales: after 12 hours at 15 K, the configurations relax only half way to equilibrium. Thus at low temperatures, the configuration populations are very stable, while they recover to equilibrium very rapidly if

the sample is heated above 35 K.

CONCLUSIONS

We have investigated the behaviour of two dominant configurations, *Conf 1* and *Conf 2*, of the Er^{3+} ion in $\text{ErSc}_2\text{N@C}_{80}$ using continuous wave EPR. The experimental spectra can be simulated to extract a spin Hamiltonian with anisotropic g - and A - and Q - tensors for each cluster configuration, to the extent allowed by the EPR linewidths. The results suggest that the erbium ion sits in a low symmetry site, at least for *Conf 1*. The two configurations are switchable through optical excitation of the C_{80} cage. The switching dynamics can be described phenomenologically by biexponential functions of time. The average decay time becomes slower at lower laser power but does not change with temperature. The recovery to equilibrium populations is very slow at low temperatures, but the equilibrium populations can be quickly recovered by annealing the sample above 35 K. This thermo-optical hysteresis makes $\text{ErSc}_2\text{N@C}_{80}$ a potential candidate for

reversible switches and memory elements [22–28].

ACKNOWLEDGEMENTS

Authors would like to thank Marshall Stoneham, William Hayes and Alexei Tyryshkin for valuable discussions. AT would like to thankfully acknowledge Dr. A. Tripathi and E. Gauger for their technical support. This research is supported by the EPSRC through the QIP IRC www.qipirc.org (No. GR/S82176/01), and the Oxford Centre of Advanced Electron Spin Resonance (No. EP/D048559/1). RR is supported by the Marie Curie QIPEST program and the EPSRC. AT is supported by Felix Scholarship. GD is supported by QIP IRC, Oxford. JJLM and AA are supported by the Royal Society. GADB is supported by EPSRC (GR/S15808/01). Un-purified TNT sample was supplied by Luna Innovations, Blacksburg, Virginia, USA.

[†] Electronic address: rizvi.rahman@materials.ox.ac.uk

[‡] Electronic address: john.morton@materials.ox.ac.uk

- [1] H. Shinohara, Rep. Prog. Phys. **63**, 843 (2000).
- [2] T. I. Smirnova, A. I. Smirnov, T. G. Chadwick, and K. L. Walker, Chem. Phys. Lett. **453**, 233 (2008).
- [3] R. M. Macfarlane, D. S. Bethune, S. Stevenson, and H. C. Dorn, Chem. Phys. Lett. **343**, 229 (2001).
- [4] L. Dunsch, M. Krause, J. Noack, and P. Georgi, J. Phys. Chem. Sol. **65**, 309 (2004).
- [5] M. Krause, H. Kuzmany, P. Georgi, L. Dunsch, K. Vietze, and G. Seifert, J. Chem. Phys. **115**, 6596 (2001).
- [6] R. Macfarlane, G. Wittmann, P. van Loosdrecht, M. de Vries, D. Bethune, S. Stevenson, and H. Dorn, Phys. Rev. Lett. **79**, 1397 (1997).
- [7] Y. Sanakis, N. Tagmatarchis, E. Aslanis, N. Ioannidis, V. Petrouleas, H. Shinohara, and K. Prassides, J. Am. Chem. Soc. **123**, 9924 (2001).
- [8] M. A. G. Jones, J. J. L. Morton, R. A. Taylor, A. Ardavan, and G. A. D. Briggs, Phys. Stat. Sol. B **243**, 3037 (2006).
- [9] A. Tiwari, G. Dantelle, K. Porfyrakis, R. A. Taylor, A. A. R. Watt, A. Ardavan, and G. A. B. Briggs, J. Chem. Phys. **127**, 194504 (2007).
- [10] A. Tiwari, G. Dantelle, K. Porfyrakis, A. Ardavan, and G. A. D. Briggs, Phys. Stat. Sol. B **245**, 1998 (2008).
- [11] M. M. Olmstead, A. de Bettencourt-Dias, J. C. Duchamp, S. Stevenson, H. C. Dorn, and A. L. Balch, J. Am. Chem. Soc. **122**, 12220 (2000).
- [12] J. J. L. Morton, A. Tiwari, G. Dantelle, K. Porfyrakis, A. Ardavan, and G. A. B. Briggs, Phys. Rev. Lett. **101**, 013002 (2008).
- [13] A. Abragam and B. Bleaney, *Electron Paramagnetic Resonance of Transition Ions* (Clarendon Press, Oxford, 1970).
- [14] S. Stoll and A. Schweiger, J. Mag. Res. **178**, 42 (2006).
- [15] M. A. G. Jones, *D. Phil. Thesis, Luminescent Erbium Metallofullerenes for Quantum Information Processing* (Department of Materials, University of Oxford, 2006).
- [16] O. Guillot-Noël, P. Goldner, Y. Du, E. Baldit, P. Monnier, and K. Bencheikh, Physical Review B **74**, 21 (2006).
- [17] J. R. Pilbrow and M. R. Lowrey, Reports on Progress in Physics **43**, 433 (1980).
- [18] M. A. G. Jones, J. J. L. Morton, R. A. Taylor, A. Ardavan, and G. A. D. Briggs, Physica Status Solidi B **243**, 3037 (2006).
- [19] F. Bloch, Phys. Rev. **70**, 460 (1946).
- [20] R. Orbach, Proc. Roy. Soc. (London) **A264**, 458 (1961).
- [21] H. J. Schneider-Muntau, B. L. Brandt, L. C. Brunel, T. A. Cross, A. S. Edison, A. G. Marshall, and A. P. Reyes, Physica B: Condensed Matter **346-347**, 643 (2004).
- [22] C. Zhang, M.-H. Du, H.-P. Cheng, X.-G. Zhang, A. E. Roitberg, and J. L. Krause, Phys. Rev. Lett. **92**, 158301 (2004).
- [23] T. Hugel, N. B. Holland, A. Cattani, L. Moroder, M. Seitz, and H. E. Gaub, Science **296**, 1103 (2002).
- [24] C. J. Nuttall, Y. Hayashi, K. Yamazaki, T. Mitani, and Y. Iwasa, Adv. Mater. **14**, 293 (2002).
- [25] M. Iwamoto, Y. Majima, H. Naruse, T. Noguchi, and H. Fuwa, Nature **353**, 645 (1991).
- [26] W. Zhao, C.-X. Wu, and M. Iwamoto, Chem. Phys. Lett. **312**, 572 (1999).
- [27] D. S. Correa, V. C. Gonçalves, D. T. Balogh, C. R. Mendonça, and L. D. Boni, Polymer **47**, 7436 (2006).
- [28] C. Berkdemir and S. Ozsoy, Opt. Comm. **254**, 248 (2005).